# Parahydrophobicity and stick-slip wetting dynamics of vertically aligned carbon nanotube forests

Ziyu Zhou [a, 1], Tongchuan Gao [b, 2], Sean McCarthy [b, 3], Andrew Kozbial [d, 3], Susheng Tan [c, 2], David Pekker [e, 2], Lei Li [d, 2], Paul W. Leu [b, *]

[a] Department of Mechanical Engineering and Materials Science, University of Pittsburgh, 3700 O'Hara St, Pittsburgh, PA, 15213, USA
[b] Department of Industrial Engineering, University of Pittsburgh, Pittsburgh, 3700 O'Hara St, Pittsburgh, PA, 15213, USA
[c] Department of Electrical and Computer Engineering, University of Pittsburgh, Pittsburgh, 3700 O'Hara St, Pittsburgh, PA, 15213, USA
[d] Department of Chemical Engineering, University of Pittsburgh, Pittsburgh, 3700 O'Hara St, Pittsburgh, PA, 15213, USA
[e] Department of Physics, University of Pittsburgh, Pittsburgh, 3700 O'Hara St, Pittsburgh, PA, 15213, USA

## ARTICLE INFO

## ABSTRACT

We report for the first time on the parahydrophobicity and stick-slip wetting dynamics of vertically aligned carbon-nanotube (CNT) forests and compare it with previously observed droplet infiltration characteristics. CNT surfaces have generally been reported to be superhydrophobic, but unstable, as the water rapidly infiltrates the forest. In this paper, we demonstrate the first observation of para-hydrophobicity of CNT forests, where the surface exhibits an apparent static water contact angle close to 150° but may be turned upside down without the droplet rolling off. Evaporation plays a critical role in the dynamic wetting behavior of these high-density samples as water droplets are stable in moisture-saturated environments. The wetting dynamics in the ambient is driven by evaporation as opposed to infiltration and characterized by contact line pinning from the strong adhesive forces in the CNTs. The pinning force at the contact line gradually increases as the droplet evaporates until a critical force is reached, where the contact line suddenly jumps radially inward with a concomitant deflection of CNTs inward. We observe that taller CNT forests have a higher critical force for deflection and coalesce into cellular patterns with larger cell size, which both suggest that taller CNTs have stronger mechanical interactions with each other.

## 1. Introduction

The application of water to vertically aligned carbon nanotube (CNT) forests may be utilized for self-assembly processes such as the densification, alignment, and folding of CNTs into foams [1,2], cellular templates [3], mutilayer assemblies [4], and densified aligned arrays [5—8]. These structures and processes may be important for a variety of applications that make use of the outstanding mechanical, electrical, and thermal properties of CNTs, such as supercapacitors [7], interconnects [9], adhesives [10], particle trapping [11], and structural color [12]. However, the dynamic wetting behavior and elastocapillary coalescence of vertically aligned CNT forests is complicated and not fully understood.

When a water droplet is placed on a vertically aligned CNT forest, the water contact angle is over 150° initially [13—15], indicative of a superhydrophobic surface. However, this high water contact angle has generally been observed to be unstable as the water droplet quickly transitions from an initial Cassie-Baxter-like state [16] to a film state within a few minutes [13—15]. This infiltration has been attributed to CNTs having a slightly hydrophilic graphitic surface with a generally accepted water contact angle of 84—86° [17—19]. After the water transitions to a film state, the water evaporates and forces the CNTs into bundles by elastocapillary coalescence [1,2,7,8,20]. Surface chemical modification of CNTs [13,21—23] or constructing micro/nano scaled hierarchical CNT films [24], has generally been found to be necessary to achieve stable superhydrophobicity.

In contrast to previously reported unstable superhydrophobicity

\* Corresponding author.
*E-mail addresses:* ziz25@pitt.edu (Z. Zhou), tog8@pitt.edu (T. Gao), stm76@pitt.edu (S. McCarthy), andrew.kozbial@gmail.com (A. Kozbial), sut6@pitt.edu (S. Tan), pekkerd@pitt.edu (D. Pekker), lel55@pitt.edu (L. Li), pleu@pitt.edu (P.W. Leu).
[1] This is the first author footnote.
[2] This is the second author footnote.
[3] This is the third author footnote.

of vertically aligned CNTs, we report on new wetting characteristics of vertically aligned CNT forests through the fabrication of high number density forests ($> 1 \times 10^{11}$ CNTs/cm$^2$). Water droplets are in fact stable for over 25 min on these high number density CNT forests in the ambient as the infiltration of water into these forests is inhibited. We present the first demonstration of para-hydyrophobicity or petal effect wetting of CNT forests, where the water contact angle is high on these CNT forests (about 150$^\circ$), but the contact angle hysteresis is large ($> 45^\circ$). These CNT forests may be turned completely upside down without the droplet rolling off, indicative of strong adhesion to the CNTs.

The wetting dynamics of these high number density CNT forests also differs drastically from the unstable behavior commonly observed in the literature. Evaporation plays a critical role in the wetting dynamics of these high number density forests as water droplets are completely stable in moisture-saturated environments. In our dynamic wetting studies, the contact line of the evaporating droplet is characterized by stick-slip behavior driven by evaporation where the contact line is pinned due to strong adhesive forces with the CNT forest and unpinned when the CNTs at the contact line are deflected radially inward. Our modeling work indicates that the change in water droplet shape and volume is consistent with evaporation governed by the diffusion of water vapor from the droplet surface. As the water droplet evaporates, the pinning force of the CNTs on the water at the contact line gradually increases until this force eventually reaches a critical force where the CNTs can no longer provide the force need to continue pinning the contact line. At this critical force, the CNTs are deflected radially inward as the contact line suddenly jumps inward. The water contact angle and baseline diameter abruptly increase and decrease, respectively, as opposed to suddenly decreasing and increasing as seen when a rapidly infiltrating droplet reaches the hydrophilic substrate. It is only after the CNT forest radially deflects inward that the water subsequently infiltrates the CNT forest rapidly. Taller CNT forests have a higher critical force for deformation, which suggests that the taller CNT forests have increased reinforcement from mechanical deformation. We also observe that the evaporation of water results in the elastocapillary coalescence of CNTs into cellular patterns where taller CNTs tend to have larger cell size, also suggestive of stronger mechanical interactions between taller CNTs. Our results offer understanding into the complex wetting of vertically aligned CNT surfaces, which may used as a CNT self assembly method for a wide variety of applications.

Furthermore, the unique parahydyrophobicity and wetting stability of high number density vertically aligned CNT forests may be adapted for various biosensing, gecko tape, water harvesting, microfluidics, and membrane devices [25–29].

## 2. Results and discussion

### 2.1. Synthesized CNTs characterization

CNT forests were synthesized by chemical vapor deposition and their wetting properties were characterized. Vertically aligned CNTs were grown from a 2 nm evaporated Fe catalyst layer on a sputtered alumina buffer layer on a Si substrate (details are provided in Supplementary Info).

Fig. 1(a) shows an (i) overhead scanning electron microscope (SEM) image and a (ii) sideview SEM image of a reference vertically aligned CNT sample, which exhibits the widely observed unstable superhydrophobicity that has been commonly reported [13–15]. Water droplets on this sample exhibit high water contact angle, but are only stable for a few minutes before the droplet transitions to a film state.

Higher number density vertically aligned CNT forests were synthesized by increasing the roughness of the alumina buffer layer. The roughness of the alumina buffer layer was increased by decreasing the distance between the alumina source and sample so that the sputtering was less isotropic. The reference sample was grown using a smoother alumina buffer layer with a root mean square (rms) roughness of 10.6 nm, while the high number density samples were grown using a rougher alumina with rms roughness of 26.5 nm (Supplementary Info, Fig. S1). The iron catalyst was annealed for 40 min prior to the introduction of an ethylene carbon source and the rougher alumina promotes the dewetting of the Fe catalyst into smaller nanoparticles that yield CNT forests with higher number density at a faster growth rate. Fig. 1(b) shows (i) overhead and (ii) side view SEM images of the high number density CNT forests. Both CNT forests were grown to a height of about 28 $\mu$m. The differences in number density in this sample are apparent from comparing its SEM images with those of the reference sample in Fig. 1(a). To estimate the number density $n$ of the aligned CNT forests, we utilized the weight-gain method [30]. Transmission electron microscopy (TEM) images (Fig. 1(c)) were used to estimate the average diameter and average number of walls of the CNTs, which were then used to estimate the number density
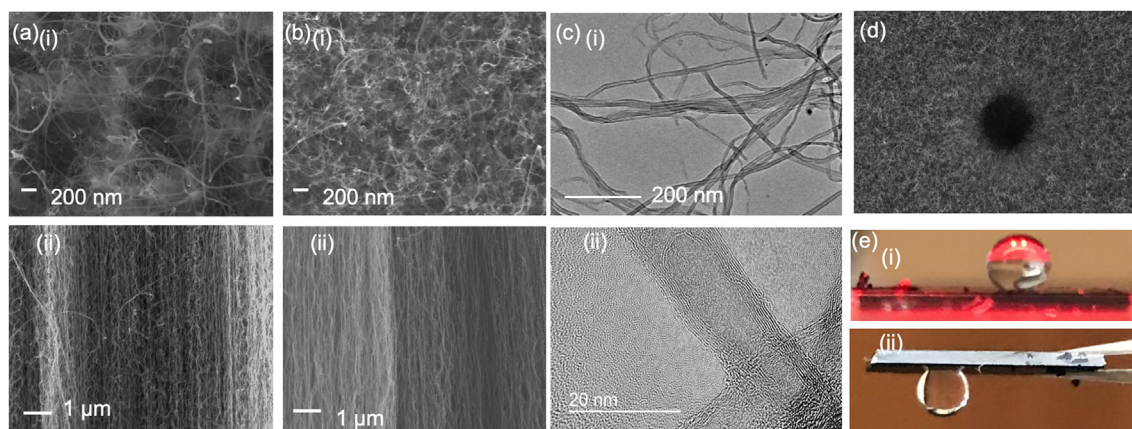


**Fig. 1.** SEM images of (a) low number density and (b) high number density vertically aligned CNT forests. (i) Overhead SEM images and (ii) sideview SEM images. (c) TEM images of tall, high number density CNTs at two different resolutions. (d) Pinholes in short, low number density CNT forest may also lead to rapid infiltration of water and droplet instability. (e) Demonstration of parahydrophobicity in high number density vertically aligned CNT forests where the droplet may be flipped upside down without rolling off in spite of the very high apparent contact angle. (A colour version of this figure can be viewed online.)

of the forests (Supplementary Info, Fig. S2). Fig. 1(c) shows TEM images of the tall, high number density CNT forest at two different resolutions. The mean outer diameter of this CNT forest is 9.7 nm and the mean number of walls is 7. The number density of the reference short, low number density sample is about $4.9 \times 10^{10}$ CNTs per $cm^2$ while the high number density sample is $13.1 \times 10^{10}$ CNTs per $cm^2$. A summary of the height, diameter, number of walls, mass density, number density, mean inter-CNT spacing, and air fraction between tubes is provided in Table S1.

The weight gain method is reliable as thermogravimetric analysis indicates our vertically aligned CNT forests consist of mainly graphitic carbon (Supplementary Info, Fig. S3) [30,31]. Additional discussion of different errors in estimating the CNT number density such as the variations in CNT diameter and number of walls as well as variations in length is provided in the Supplementary Info. The higher number density samples have better alignment as characterized by the Hermann Orientation Factor (calculated in the Supplementary Info) due to the crowding effect [32]. The higher number density CNT forests tend to not only be more compacted, but better aligned, and more uniformly distributed across the sample. This higher number density and higher uniformity both provide for better water droplet stability as the lower mean inter-CNT spacing and lower variation in CNT-spacing more strongly inhibits the infiltration of water into the CNT forest.

In addition to the worse uniformity in the lower number density reference sample, pinholes such as that shown in Fig. 1(d) also lead to the rapid infiltration of water into the forest such that the water droplet collapses within a few seconds and quickly transitions into a film state. These pinholes may form if there are particulates present on the catalyst.

## 2.2. Characterization of CNTs wetting behavior

Water droplets on the low number density reference forest are relatively unstable as have been commonly observed in the literature [13–15]. However, water droplets on the high number density forest are stable in atmosphere and enables additional characterization. Quite surprisingly, the high number density CNT forest exhibits parahydrophobicity [26] where the water contact angle is high (Fig. 1(e),i), but the droplet also has strong adhesion such that the droplet remains adhered to the surface even when it is tilted upside down (Fig. 1(e),ii). The droplet adheres to the surface even after the CNT forest has been inverted immediately after water deposition (see Video S1 in the Supplementary Info). Table 1 summarizes our wetting characterization results based on characterization of three droplets on each sample. The high number density exhibits a large hysteresis angle or difference between advancing and receding angle, which is indicative of strong adhesion.

Supplementary video related to this article can be found at https://doi.org/10.1016/j.carbon.2019.06.012.

This wetting behavior of high contact angle together with strong adhesion is also referred to as petal effect wetting [33,34] as rose petals exhibit this type of wetting and is distinct from lotus effect wetting, where high water contact angle droplets have low

adhesion and easily bounce or roll off the surface [35]. Petal effect wetting has also been observed in gecko feet [36] and peach skin [37]. Hierarchical structures [38] as well as polymer nanotubes [29,39] have also demonstrated this type of wetting. Parahydrophobicity may be explained by a metastable intermediate state of wetting between the Wenzel or Cassie-Baxter regime referred to as the Cassie-Impregnating regime [38], where some surface features exhibit Wenzel wetting and others exhibit Cassie-Baxter behavior [40,41]. In CNTs, the Cassie-Impregnating state may occur because the surface of graphitic carbon has been shown to be intrinsically mildly hydrophilic, but becomes hydrophobic after airborne hydrocarbon contamination [42,43]. This heterogeneity of both hydrophilic and hydrophobic regions in CNTs may provide for the parahydrophobicity observed [26].

Next, we performed dynamic wetting studies on three different CNT samples, which are summarized in Fig. 2. Fig. 2(a) shows the change of the baseline or contact area diameter with time. The high number density samples show distinct behavior from the low number density reference sample. The contact areas of the water droplet on the CNT forests is mostly constant due to the strong adhesion forces discussed above and the contact lines are characterized by abrupt and sudden changes. While the water droplet on the low number density sample shows a sudden increase in baseline diameter after only about 3 min, the high number density samples are stable for over 25 min, after which the baseline diameter suddenly decreases.

Notably, the short, high number density forest experiences two sudden decreases in baseline diameter, while the tall, high number density forest experiences one sudden decrease. Fig. 2(b) shows optical images of the water droplet for the three types of samples. Images are taken at 2 min intervals for the reference sample and at 6 min intervals for the high number density forests, where the contact area diameter is marked by red lines. Fig. 2(c) plots the water contact angle of the three different samples as a function of time. As the water droplet evaporates, the water contact angle decreases gradually. For the low number density sample, the water contact angle abruptly drops from 150 to 50° after about 3 min. The contact line is pinned again at about 50° after this sudden jump and evaporation is again responsible for the continuous decline in water contact angle. For the high number density samples, the contact angles also decrease initially due to evaporation. The contact angles between the two samples begin to deviate after about 23 min. This may be due to the slight differences in number density discussed earlier between the two samples or slight differences in the environment. We additionally model the contact angle change with time using an evaporation model in which the rate at which the droplet loses water is governed by the diffusion of the water vapor from the surface of the droplet [44]. Details of this model and how this model is solved numerically are described in the Supplementary Info. The results of this model are shown in Fig. 2(c) with the cyan and pink dashed lines for the short, high number density and tall, high number density samples, respectively. As can be seen, the decrease in water contact angle of these two high number density samples generally follow that due to evaporation until there is a sudden increase in water contact angle. For the short, high number density sample, the contact angle jumps from 41° up to 81° at about 25 min and then again from 63° up to 79° at about 26 min. The tall, high number density samples experience a similar abrupt increase in water contact angle, though this happens at a much smaller water contact angle. The water contact angle jumps from 6° to 9° after most of the droplet has evaporated. Videos S2–S4 showing the water droplet evolution of the three different types of CNT samples are included in the Supplementary Info. Another video (S5) showing the wetting dynamics of the three samples concurrently is also including the Supplementary Info.

**Table 1**
Summary of contact angle results of CNTs with water droplet.

| Sample | Reference (°) | High n (°) |
|---|---|---|
| Static Contact Angle ($\theta_s$) | 152.3 ± 0.1 | 146.5 ± 0.1 |
| Advancing Angle ($\theta_a$) | | 149.7 ± 0.4 |
| Receding Angle ($\theta_r$) | | 103.8 ± 4.7 |
| Hysteresis Angle ($\theta_h$) | | 45.9 ± 4.3 |
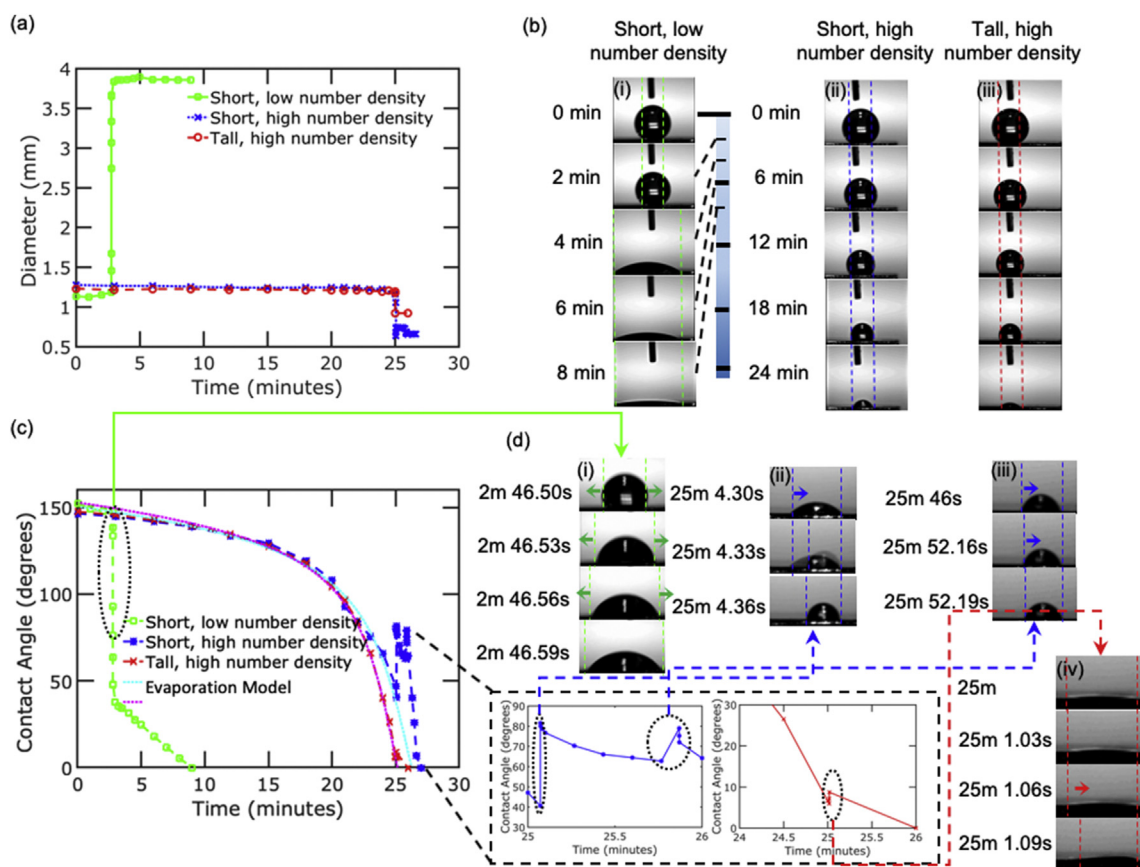
**Fig. 2.** CNT wetting dynamics in the ambient. (a) Baseline diameter versus time. (b) Optical microscope images of water droplets over time. (c) Water contact angle as a function of time for three types of samples Enlarged image shows the contact angle changing details for tall, high number density sample. (d) Enlarged frame by frame optical microscope images of contact angle change with time for (i) short, low number density and (ii) short, high number density CNT forests. (A colour version of this figure can be viewed online.)

Supplementary video related to this article can be found at https://doi.org/10.1016/j.carbon.2019.06.012.

SEM images of the aligned CNT forests were taken after wetting experiments (Fig. 3), which reveal very different CNT assembly patterns. Cellular patterns of aggregated CNTs are seen in the low number density sample similar to those commonly reported [14,15]. In contrast, the high number density sample shows a ring-like pattern where the original contact line was pinned. We note the CNTs are also deflected radially inward at this contact line corresponding to the sudden jump inward of the contact line after 25 min. In the short, high number density samples, a second concentric ring may be observed which likely coincides with the second jump inward observed. Cellular patterns may be observed throughout the sample similar to the reference sample due to evaporation of the water after the water has formed a film. In contrast, the tall, high number density sample primarily has cellular patterns within the original contact line. There is some evidence of water infiltrating beyond this initial contact line, but the extent of this infiltration is limited. We also note that the cellular patterns in the tall CNT forest are larger than those in the two short CNT forests, which have comparable cell size.

We further studied wetting in a moisture-saturated environment to eliminate the role of evaporation. Fig. 4 presents the results of experiments on the short and tall, high number density samples. Wetting tests were also performed on the reference sample but the wetting behavior was like that in the ambient environment, suggesting that evaporation does not play a critical role in the transition of the droplet into a film state in the low number density CNT sample. Details of how these experiments were performed may be

found in the Methods section and an accompanying schematic may be found in the Supplementary Info, Fig. S5. In contrast, the water droplet contact angles on high number density samples are stable between 140° and 150° over 3 days, revealing the critical role of evaporation in CNT wetting dynamics in the ambient. Optical pictures shown in Fig. 4(b) reveal no change in the water droplet and the contact lines remain fixed. Finally, after 72 h, the water droplet was wicked away. SEM images in Fig. 4(c) reveal that capillary forces have bundled the CNTs together into one central array. The rapid wicking away process of water from the center promotes the formation of this single array as opposed to the cellular patterns formed during evaporation in the ambient environment (Fig. 4(c), ii compared to Fig. 3(c),i). The cellular bundles in the shorter CNTs are smaller in Fig. 3(b)(i), while all the CNTs in the tall forest have been bundled together at the center in Fig. 3(c)(i). We also observe some water infiltration beyond the contact line in the short, high number density forests due the short height of CNT sample. This suggests that downward water infiltration still occurs in these samples, but at a much slower rate.

### 2.3. Mechanism of CNTs wetting

Based on our experiments, we create a schematic illustrating the wetting process for different CNT forests in the ambient as shown in Fig. 5. The water droplet in all three samples exists in a meta-stable Cassie-Baxter-like state with air trapped underneath (Fig. 5(i)). Droplets gradually (1) infiltrate downward into the forest as the droplet transitions from a Cassie-Baxter-like state to a Wenzel-like state through so called Cassie-Impregnating states and
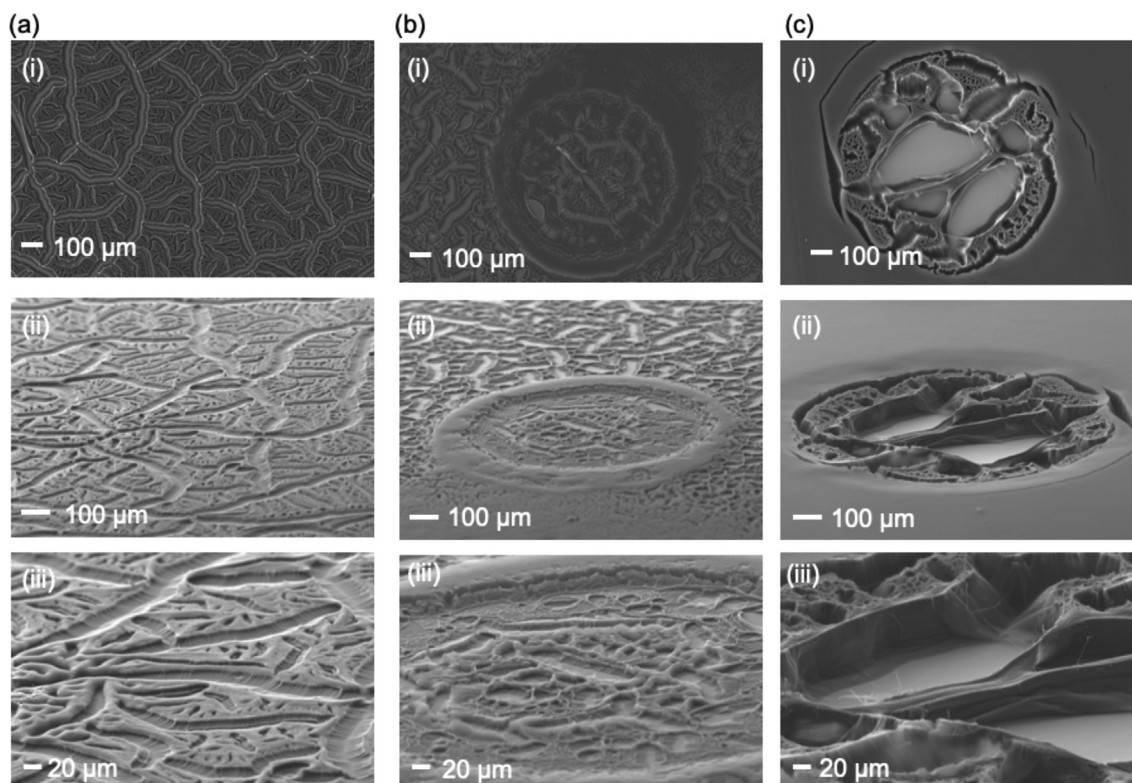
**Fig. 3.** SEM images of wetting patterns for (a) short, low number density, (b) short, high number density, and (c) tall, high number density aligned CNT forests. (i) Overhead SEM images and (ii, iii) tilted at 70° from overhead SEM images are shown.
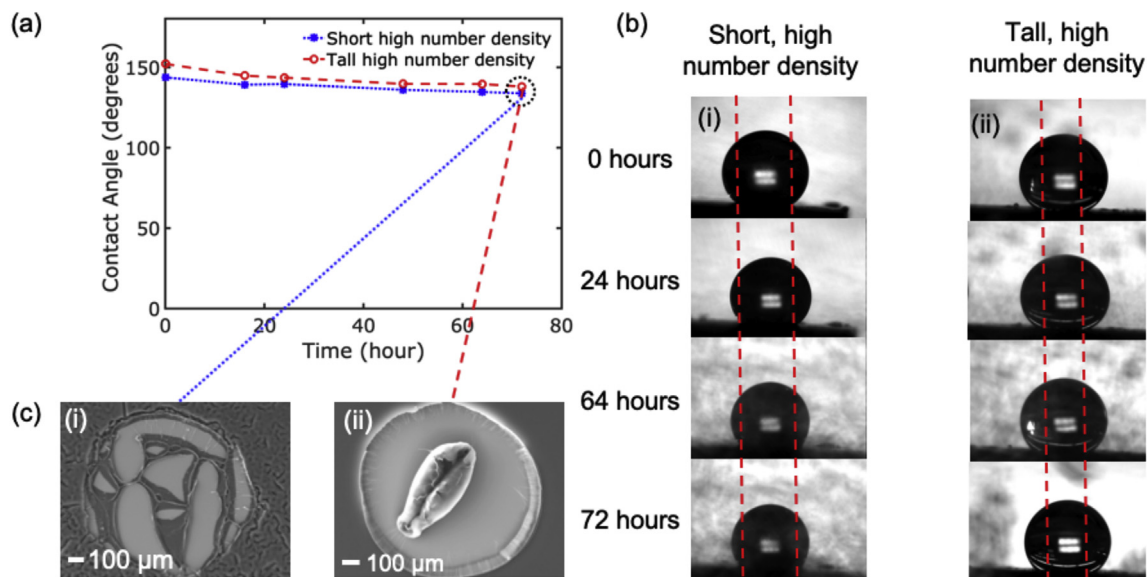


**Fig. 4.** (a) SEM images of wetting patterning under different environments in the ambient environment (blue dot line) and in the saturated environment (red dash line). (b) Optical images for long-term stability test for (i) short high number density sample and (ii) tall high number density sample. (c) SEM images for (i) short high number density sample and (ii) tall high number density sample after 72 h stability test. (A colour version of this figure can be viewed online.)

(2) evaporate which increases the pinning force of the CNTs on the water at the water contact line (Fig. 5ii).

The three phase contact line is pinned while these processes happen due to the strong adhesion of the water droplet with the CNT forests. Two types of abrupt transitions occur in these samples (Fig. 5iii). In the low number density sample, this jump occurs when the maximum infiltration reaches the hydrophilic substrate. The abrupt transition has been previously reported for micropillars of PDMS [45]. The droplet suddenly changes into a film state (Fig. 5(a),iv) and the subsequent evaporation bundles the tubes into cellular patterns (Fig. 5(a),v and vi). On the other hand, the water infiltration in the high number density samples occurs much more
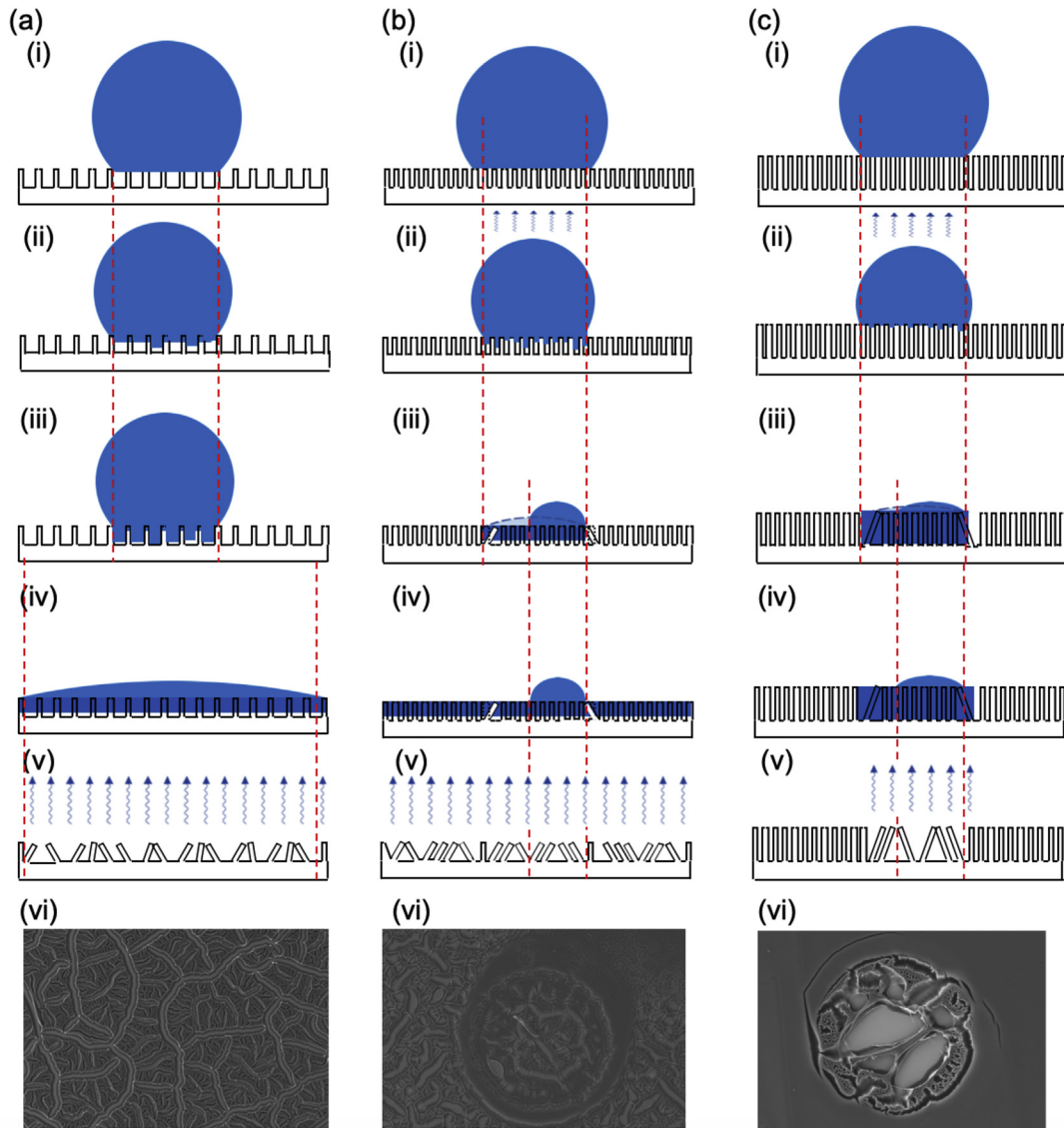
**Fig. 5.** Schematic of wetting process for three CNT samples: (a) short, low number density, (b) short, high number density, and (c) tall, high number density, aligned CNT forests. (i) original water droplet on the sample, (ii) evaporation and infiltration happens, (iii) critical states (water touches the bottom or critical force reached), (iv) wetting and evaporation, (v) elastocapillary coalesecence and (vi) SEM images of surface after evaporation. (A colour version of this figure can be viewed online.)

slowly. Instead, evaporation gradually decreases the droplet size and the droplet contact angle. An abrupt transition occurs when the pinning force on the contact line reaches a critical CNT deflection force, where the CNTs can no longer provide the force required to continue pinning the contact line. The CNTs are deflected radially inward as the water contact line jumps and this allows water to flow into the forest (Fig. 5(b),iv) and rapidly achieve a film state (Fig. 5(b),v). This type of stick-slip behavior has been previously reported for nanoparticle suspensions, which may experience multiple slip events with associated deposition of nanoparticles into rings [46,47]. In contrast, we observe a maximum of two slip events in our wetting dynamic studies due to the deflection of CNTs and subsequent infiltration of water into the CNT forests. Evaporation of the droplet again forms cellular patterns due to elasto-capillary coalescence where capillary forces cause the CNTs to adhere to nearby CNTs [48] (Fig. 5(b),v and vi). The tall, high density CNT forests also undergo the same abrupt transition at a critical force, but this transition occurs when the water is almost completely evaporated such that there is limited infiltration of the

water outside the original contact line. We estimate the critical force on the two high number density forests when the abrupt deflection of CNTs occurs. The force per unit length on the contact line is

$$F = \gamma_{LA}(\cos \theta - \cos\theta_{eq}) \qquad (1)$$

where $\gamma_{LA} = 72.8$ mN/m is the surface tension of water, $\theta_{eq}$ is the equilibrium water contact angle and $\theta$ is the water contact angle at any time. The critical force $F_c$ is calculated from the critical water contact angle $\theta_c$, when the water contact line suddenly jumps inward. The critical force is 3.2 nN and 4.0 nN per CNT for the short, high number density and tall, high number density samples, respectively. Elastocapillary theory, where CNTs are treated like independent beams, suggests that longer CNTs should buckle at lower critical forces [4]. In contrast, the longer CNTs in our experiments deform at higher critical forces suggesting that taller CNTs have stronger reinforcement from deformation, which may be due to increased van der Waals forces from contact or entanglement

interactions between neighboring CNTs [49]. We also note that the tall CNT forests have larger cell sizes after evaporation than the two short CNT forests, which further supports that taller CNTs have increased mechanical interactions with their neighbors.

## 3. Conclusions

We fabricated high number density ($> 1 \times 10^{11}$ CNTs/cm$^2$) CNT forests, which provide for increased wetting stability compared to CNTs commonly reported in the literature. We offer the first demonstration of parahydrophobicity on high number density CNT forests, where the water contact angle is about $150°$, but the contact angle hysteresis is $> 45°$. These vertically aligned CNT forests may be turned upside down without the droplet rolling off. We also studied the wetting dynamics of high number density CNT forests of different height and compared them to the unstable super-hydrophobicity of the reference sample. The high number density vertically aligned CNT forests demonstrate water droplet stability over 25 min in an ambient environment and over three days in a saturated environment, revealing the critical role of evaporation in ambient wetting dynamics. The water droplet dynamics in these high number density samples is governed by stick-slip behavior due to evaporation of the water droplet as opposed to the downward water infiltration into the forest. Above a critical pinning force, the contact line suddenly jumps and the CNTs at the contact line deform radially inward. This initiates the infiltration process by which the water contact angle rapidly decreases. These results offer understanding into the complex wetting of vertically aligned CNT surfaces, which may used as a self assembly method for the densification, alignment, and folding of CNTs for applications such as supercapacitors, interconnects, adhesives, particle trapping, and structural color. The unique parahydrophobicity properties of CNTs reported here could potentially be used in combination with the other excellent mechanical, thermal, and electrical properties of CNTs.

## Acknowledgements

## Appendix A. Supplementary data

Supplementary data to this article can be found online at https://doi.org/10.1016/j.carbon.2019.06.012.

## References

[1] N. Chakrapani, B. Wei, A. Carrillo, P.M. Ajayan, R.S. Kane, Capillarity-driven assembly of two-dimensional cellular carbon nanotube foams, Proc. Natl. Acad. Sci. Unit. States Am. 101 (12) (2004) 4009–4012, https://doi.org/10.1073/pnas.0400734101. http://www.pnas.org/content/101/12/4009.

[2] C.T. Wirth, S. Hofmann, J. Robertson, Surface properties of vertically aligned carbon nanotube arrays, Diam. Relat. Mater. 17 (7–10) (2008) 1518–1524, https://doi.org/10.1016/j.diamond.2007.11.019. http://www.sciencedirect.com/science/article/pii/S0925963507004979.

[3] P.M. Ajayan, O. Stephan, P. Redlich, C. Colliex, Carbon nanotubes as removable templates for metal oxide nanocomposites and nanostructures, Nature 375 (6532) (1995), https://doi.org/10.1038/375564a0, 375564a0, https://www.nature.com/articles/375564a0.

[4] S. Tawfick, M. De Volder, A.J. Hart, Structurally programmed capillary folding of carbon nanotube assemblies, Langmuir 27 (10) (2011) 6389–6394.

[5] M.F. De Volder, S.J. Park, S.H. Tawfick, D.O. Vidaud, A.J. Hart, Fabrication and electrical integration of robust carbon nanotube micropillars by self-directed elastocapillary densification, J. Micromech. Microeng. 21 (4) (2011), 045033.

[6] E. Garcia, A. Hart, B. Wardle, A. Slocum, Fabrication of composite microstructures by capillarity-driven wetting of aligned carbon nanotubes with polymers, Nanotechnology 18 (16) (2007) 165602.

[7] D.N. Futaba, K. Hata, T. Yamada, T. Hiraoka, Y. Hayamizu, Y. Kakudate, O. Tanaike, H. Hatori, M. Yumura, S. Iijima, Shape-engineerable and highly densely packed single-walled carbon nanotubes and their application as super-capacitor electrodes, Nat. Mater. 5 (12) (2006) 987–994.

[8] Z. Liu, N. Bajwa, L. Ci, S. Lee, S. Kar, P. Ajayan, J.-Q. Lu, Densification of carbon nanotube bundles for interconnect application, in: International Interconnect Technology Conference, IEEE 2007, IEEE, 2007, pp. 201–203.

[9] M.F. De Volder, S.J. Park, S.H. Tawfick, D.O. Vidaud, A.J. Hart, Fabrication and electrical integration of robust carbon nanotube micropillars by self-directed elastocapillary densification, J. Micromech. Microeng. 21 (4) (2011), 045033.

[10] B. Pokroy, S.H. Kang, L. Mahadevan, J. Aizenberg, Self-organization of a mesoscale bristle into ordered, hierarchical helical assemblies, Science 323 (5911) (2009) 237–240, https://doi.org/10.1126/science.1165607, arXiv: http://science.sciencemag.org/content/323/5911/237.full.pdf, http://science.sciencemag.org/content/323/5911/237. URL.

[11] D. Wu, S.-Z. Wu, S. Zhao, J. Yao, J.-N. Wang, Q.-D. Chen, H.-B. Sun, Rapid, controllable fabrication of regular complex microarchitectures by capillary assembly of micropillars and their application in selectively trapping/releasing microparticles, Small 9 (5) (2012) 760–767, https://doi.org/10.1002/smll.201201689. https://onlinelibrary.wiley.com/doi/abs/10.1002/smll.201201689.

[12] D. Chandra, S. Yang, A.A. Soshinsky, R.J. Gambogi, Biomimetic ultrathin whitening by capillary-force-induced random clustering of hydrogel micropillar arrays, ACS Appl. Mater. Interfaces 1 (8) (2009) 1698–1704, https://doi.org/10.1021/am900253z. https://doi.org/10.1021/am900253z.

[13] K.K.S. Lau, J. Bico, K.B.K. Teo, M. Chhowalla, G.A.J. Amaratunga, W.I. Milne, G.H. McKinley, K.K. Gleason, Superhydrophobic carbon nanotube forests, Nano Lett. 3 (12) (2003) 1701–1705, https://doi.org/10.1021/nl034704t. https://doi.org/10.1021/nl034704t.

[14] H. Liu, J. Zhai, L. Jiang, Wetting and anti-wetting on aligned carbon nanotube films, Soft Matter 2 (10) (2006) 811–821, https://doi.org/10.1039/B606654B. http://pubs.rsc.org/en/content/articlelanding/2006/sm/b606654b.

[15] H. Liu, S. Li, J. Zhai, H. Li, Q. Zheng, L. Jiang, D. Zhu, Self-assembly of large-scale micropatterns on aligned carbon nanotube films, Angew. Chem. Int. Ed. 43 (9) (2004) 1146–1149, https://doi.org/10.1002/anie.200351988. http://onlinelibrary.wiley.com/doi/10.1002/anie.200351988/abstract.

[16] A.B.D. Cassie, S. Baxter, Wettability of porous surfaces, Trans. Faraday Soc. 40 (1944) 546, https://doi.org/10.1039/tf9444000546. http://pubs.rsc.org/en/Content/ArticleLanding/1944/TF/tf9444000546.

[17] A.H. Barber, R. Andrews, L.S. Schadler, H.D. Wagner, On the tensile strength distribution of multiwalled carbon nanotubes, Appl. Phys. Lett. 87 (2005) 203106, https://doi.org/10.1063/1.2130713. http://link.aip.org/link/APPLAB/v87/i20/p203106/s1&Agg=doi.

[18] F.M. Fowkes, Attractive forces at interfaces, Ind. Eng. Chem. 56 (12) (1964) 40–52, https://doi.org/10.1021/ie50660a008. https://doi.org/10.1021/ie50660a008.

[19] F.M. Fowkes, W.D. Harkins, The state of monolayers adsorbed at the interface solid—aqueous solution, J. Am. Chem. Soc. 62 (12) (1940) 3377–3386, https://doi.org/10.1021/ja01869a029, 00208, https://doi.org/10.1021/ja01869a029.

[20] P.M. Ajayan, S. Iijima, Capillarity-induced filling of carbon nanotubes, Nature 361 (6410) (1993) 333–334, https://doi.org/10.1038/361333a0. https://doi.org/10.1038/361333a0.

[21] S. Abraham, G. Ma, C.D. Montemagno, Janus carbon nanotube membranes by selective surface plasmoxidation, Adv. Mater. Interfaces 3 (18) (2016).

[22] B. Li, J. Zhang, Polysiloxane/multiwalled carbon nanotubes nanocomposites and their applications as ultrastable, healable and superhydrophobic coatings, Carbon 93 (2015) 648–658.

[23] S. Hong, M.Y. Chou, Effect of hydrogen on the surface-energy anisotropy of diamond and silicon, Phys. Rev. B 57 (11) (1998) 6262–6265.

[24] P. Wang, T. Zhao, R. Bian, G. Wang, H. Liu, Robust superhydrophobic carbon nanotube film with Lotus leaf mimetic multiscale hierarchical structures, ACS Nano 11 (12) (2017) 12385–12391, https://doi.org/10.1021/acsnano.7b06371. https://doi.org/10.1021/acsnano.7b06371.

[25] A.K. Geim, S.V. Dubonos, I.V. Grigorieva, K.S. Novoselov, A.A. Zhukov, S.Y. Shapoval, Microfabricated adhesive mimicking gecko foot-hair, Nat. Mater. 2 (7) (2003) 461–463, https://doi.org/10.1038/nmat917. https://doi.org/10.1038/nmat917.

[26] C.R. Szczepanski, F. Guittard, T. Darmanin, Recent advances in the study and design of parahydrophobic surfaces: from natural examples to synthetic approaches, Adv. Colloid Interface Sci. 241 (2017) 37–61. https://www.sciencedirect.com/science/article/pii/S0001868616302780.

[27] J. Li, Z. Jing, F. Zha, Y. Yang, Q. Wang, Z. Lei, Facile spray-coating process for the fabrication of tunable adhesive superhydrophobic surfaces with heterogeneous chemical compositions used for selective transportation of microdroplets with different volumes, ACS Appl. Mater. Interfaces 6 (11) (2014) 8868–8877.

[28] X. Hong, X. Gao, L. Jiang, Application of superhydrophobic surface with high adhesive force in no lost transport of superparamagnetic microdroplet, J. Am. Chem. Soc. 129 (6) (2007) 1478–1479.

[29] T. Darmanin, F. Guittard, A one-step electrodeposition of homogeneous and vertically aligned nanotubes with parahydrophobic properties (high water adhesion), J. Mater. Chem. 4 (9) (2016) 3197–3203.

[30] S. Esconjauregui, R. Xie, M. Fouquet, R. Cartwright, D. Hardeman, J. Yang,

J. Robertson, Measurement of area density of vertically aligned carbon nanotube forests by the weight-gain method, J. Appl. Phys. 113 (14) (2013) 144309.

[31] N. Chiodarelli, O. Richard, H. Bender, M. Heyns, S. De Gendt, G. Groeseneken, P.M. Vereecken, Correlation between number of walls and diameter in multiwall carbon nanotubes grown by chemical vapor deposition, Carbon 50 (5) (2012) 1748—1752, https://doi.org/10.1016/j.carbon.2011.12.020. http://www.sciencedirect.com/science/article/pii/S0008622311009651.

[32] M. Xu, D.N. Futaba, M. Yumura, K. Hata, Alignment control of carbon nanotube forest from random to nearly perfectly aligned by utilizing the crowding effect, ACS Nano 6 (7) (2012) 5837—5844. https://pubs.acs.org/doi/abs/10.1021/nn300142j.

[33] J.B.K. Law, A.M.H. Ng, A.Y. He, H.Y. Low, Bioinspired ultrahigh water pinning nanostructures, Langmuir 30 (1) (2014) 325—331.

[34] L. Feng, Y. Zhang, J. Xi, Y. Zhu, N. Wang, F. Xia, L. Jiang, Petal effect: a superhydrophobic state with high adhesive force, Langmuir 24 (8) (2008) 4114—4119.

[35] W. Barthlott, C. Neinhuis, Purity of the sacred lotus, or escape from contamination in biological surfaces, Planta 202 (1) (1997) 1—8, https://doi.org/10.1007/s004250050096. http://www.springerlink.com/content/4m4jnt03qlvaywjl/.

[36] K. Liu, J. Du, J. Wu, L. Jiang, Superhydrophobic gecko feet with high adhesive forces towards water and their bio-inspired materials, Nanoscale 4 (3) (2012) 768—772.

[37] X. Lu, H. Cai, Y. Wu, C. Teng, C. Jiang, Y. Zhu, L. Jiang, Peach skin effect: a quasi-superhydrophobic state with high adhesive force, Sci. Bull. 60 (4) (2015) 453—459.

[38] B. Bhushan, M. Nosonovsky, The rose petal effect and the modes of superhydrophobicity, Phil. Trans. Ser. A Math. Phys. Eng. Sci. 368 (1929) (2010) 4713—4728, https://doi.org/10.1098/rsta.2010.0203.

[39] M. Jin, X. Feng, L. Feng, T. Sun, J. Zhai, T. Li, L. Jiang, Superhydrophobic aligned polystyrene nanotube films with high adhesive force, Adv. Mater. 17 (16) (2005) 1977—1981.

[40] L. Feng, Y. Zhang, J. Xi, Y. Zhu, N. Wang, F. Xia, L. Jiang, Petal effect: a superhydrophobic state with high adhesive force, Langmuir 24 (8) (2008) 4114—4119, https://doi.org/10.1021/la703821h. https://doi.org/10.1021/la703821h.

[41] Y. Lai, J. Huang, Z. Cui, M. Ge, K.-Q. Zhang, Z. Chen, L. Chi, Recent advances in TiO2 -based nanostructured surfaces with controllable wettability and adhesion, Small (Weinheim an Der Bergstrasse, Germany) 12 (16) (2016) 2203—2224, https://doi.org/10.1002/smll.201501837.

[42] Y. Gogotsi, J.A. Libera, A. Güvenç-Yazicioglu, C.M. Megaridis, In situ multiphase fluid experiments in hydrothermal carbon nanotubes, Appl. Phys. Lett. 79 (7) (2001) 1021—1023, https://doi.org/10.1063/1.1391228. https://aip.scitation.org/doi/abs/10.1063/1.1391228.

[43] Z. Li, Y. Wang, A. Kozbial, G. Shenoy, F. Zhou, R. McGinley, P. Ireland, B. Morganstein, A. Kunkel, S.P. Surwade, L. Li, H. Liu, Effect of airborne contaminants on the wettability of supported graphene and graphite, Nat. Mater. 12 (10) (2013) 925.

[44] H. Hu, R.G. Larson, Evaporation of a sessile droplet on a substrate, J. Phys. Chem. B 106 (6) (2002) 1334—1344.

[45] S. Moulinet, D. Bartolo, Life and death of a fakir droplet: impalement transitions on superhydrophobic surfaces, Eur. Phys. J. E 24 (3) (2007) 251—260, https://doi.org/10.1140/epje/i2007-10235-y. https://link.springer.com/article/10.1140/epje/i2007-10235-y.

[46] J.R. Moffat, K. Sefiane, M.E.R. Shanahan, Effect of TiO2 nanoparticles on contact line stick-slip behavior of volatile drops, J. Phys. Chem. B 113 (26) (2009) 8860—8866, https://doi.org/10.1021/jp902062z. https://doi.org/10.1021/jp902062z.

[47] D. Orejon, K. Sefiane, M.E.R. Shanahan, Stick—slip of evaporating droplets: substrate hydrophobicity and nanoparticle concentration, Langmuir 27 (21) (2011) 12834—12843, https://doi.org/10.1021/la2026736. https://doi.org/10.1021/la2026736.

[48] J. Bico, B. Roman, L. Moulin, A. Boudaoud, Adhesion: elastocapillary coalescence in wet hair, Nature 432 (7018) (2004) 690.

[49] M. Bedewy, E.R. Meshot, H. Guo, E.A. Verploegen, W. Lu, A.J. Hart, Collective mechanism for the evolution and self-termination of vertically aligned carbon nanotube growth, J. Phys. Chem. C 113 (48) (2009) 20576—20582, https://doi.org/10.1021/jp904152v. https://doi.org/10.1021/jp904152v.